

Electronic Supplementary Information

Predicting DNP-SENS Efficiency in Reactive Heterogeneous Catalysts from Hydrophilicity.

Eva Pump,^a Anissa Bendjeriou-Sedjerari,^a Jasmine Viger-Gravel,^b David Gajan,^c Baptiste Scotto,^a Manoja K. Samantaray,^a Edy Abou-Hamad,^d Andrei Gurinov,^d Walid Almaksoud,^a Zhen Cao,^a Anne Lesage,^c Luigi Cavallo,^a Lyndon Emsley*^b and Jean-Marie Basset**^a

^[a] KAUST Catalysis Center (KCC), King Abdullah University of Science and Technology, Thuwal, 23955-6900, Saudi Arabia

^[b] Institut des Sciences et Ingénierie Chimiques, Ecole Polytechnique Fédérale de Lausanne (EPFL), CH-1015 Lausanne, Switzerland

^[c] Institut de Sciences Analytiques (CNRS / ENS-Lyon / UCB-Lyon 1), Université de Lyon, Centre de RMN à Très Hauts Champs, 69100 Villeurbanne, France

^[d] King Abdullah University of Science and Technology (KAUST), Core Labs, Thuwal, 23955-6900, Saudi Arabia

Table of contents

1. General Procedure	2
2. Sample Preparation	2
3. Fourier Transformed Infrared spectroscopy (FTIR)	3
4. Elemental analyses and inductively coupled plasma optical emission spectrometry (ICP-OES)	4
5. Nitrogen adsorption/desorption measurements	5
6. Transmission-electron microscopy (TEM)	6
7. Computational Methods	7
8. Dynamic Nuclear Polarization Surface Enhanced NMR spectroscopy (DNP SENS)	8
9. EPR spectroscopy	14
10. References	15

1. General Procedure

All experiments were carried out under controlled atmosphere. Treatments of the surface species were carried out using high vacuum lines (10^{-5} mbar) and glove box techniques. SiO_{2-700} **0** was prepared from commercial available silica (Aerosil-200) from Degussa ($d_{\text{silica}} = 15$ nm), which were partially dehydroxylated at 700°C under high vacuum ($< 10^{-5}$ mbar) for 24 hours to give a white solid having a specific surface area of $183 \text{ m}^2/\text{g}$ and containing $0.3 \text{ OH}/\text{nm}^2$.^{1,2} *n*-Pentane was distilled on Na - benzophenone and degassed through freeze pump thaw cycles. $\text{Ti}(\text{CH}_2^t\text{Bu})_4$ **I**, $\text{Zr}(\text{CH}_2^t\text{Bu})_4$ **II**, WMe_6 **III** and $\text{Ga}(\text{iBu})_3$ were prepared according to literature.²⁻⁶ $\text{W}(\equiv\text{C}^t\text{Bu})(\text{CH}_2^t\text{Bu})_3$ **IV** was purchased from Strem. Chemical and sublimed prior to usage at 60°C under vacuum ($< 10^{-5}$ mbar) obtaining a yellow powder. ZnMe_2 (1M in heptane) **V** was ordered from Sigma Aldrich. TEKPol⁷ was dried under high vacuum (10^{-4} mbar) and the solvents were stirred over calcium hydride, distilled and degassed.

2. Sample Preparation

Grafting of organometallic complexes [$\text{Ti}(\text{CH}_2^t\text{Bu})_4$ **I**, $\text{Zr}(\text{CH}_2^t\text{Bu})_4$ **II**, WMe_6 **III**, $\text{W}(\equiv\text{C}^t\text{Bu})(\text{CH}_2^t\text{Bu})_3$ **IV**, ZnMe_2 **V** and $\text{Ga}(\text{iBu})_3$ **VI**] on silica₇₀₀ was performed according to literature.^{2, 6, 8-10}

For materials **1**, **2**, **4** and **6**, SiO_{2-700} **0** (1.0 g) was suspended in *n*-pentane (6 mL) in a reactor. The respective amount of organometallic catalyst leading to 0.2 (**low**), 0.4 (**med**) and 1.0 eq [SOMF]/g of eg. $[\equiv\text{SiOH}]$ (**high**) was dissolved in *n*-pentane (4 mL) was added and stirred under Argon atmosphere overnight under exclusion of light leading to **1-med**, **1-low**, **2-med**, **2-low**, **4-high**, **4-med**, **4-low**, **6-high**, and **6-med**, respectively. After completion of the reaction (20 h), the supernatant was removed and the material was washed three times with fresh *n*-pentane.

For **3**, SiO_{2-700} **0** (500 mg) was suspended in *n*-pentane (20 mL) in a double Schlenk. A solution of WMe_6 **III** in *n*-pentane was added and reacted at -40°C for 2 h (**2-low**) or 6 h (**2-med**). Then, the solvent was removed by filtration, the precipitate was washed with *n*-pentane.

For **5**, SiO_{2-700} **0** (1.0 g) was suspended in *n*-pentane (10 mL) in a reactor. The appropriate amount of a ZnMe_2 -solution in *n*-heptane ($c = 1\text{M}$) was added and reacted overnight at RT leading to **5-low** and **5-med**. Afterwards, the solvent was removed by filtration and the precipitate was washed with *n*-pentane.

The samples were dried in high vacuum (10^{-5} mbar) and stored at -40°C under argon atmosphere in a glovebox.

Trimethylsilyl-functionalization of SiO_{2-700} **0** was prepared according to literature.¹¹ SiO_{2-700} **0** (1 g) was suspended in toluene (25 mL) and hexamethyldisilazane (HDMS) (380 μL) was added. The reaction was stirred overnight at 80°C . Then, the remaining toluene was filtered and the silica was washed three times and dried in vacuo, leading to **0-high**.

3. Fourier Transformed Infrared spectroscopy (FTIR)

Spectra were acquired on a Nicolet 6700 FT-IR spectrometer equipped with a cell under controlled atmosphere. The FT-IR spectrum of (**4-high**) shows a strong decrease of the intensity of the $\nu(\text{OH})$ band at 3749 cm^{-1} , which is in accordance with elemental analysis suggesting that around 80% of all $[\equiv\text{SiOH}]$ groups have reacted. This decrease is associated with the appearance of neopentyl-moieties in the region between $3012\text{-}2727\text{ cm}^{-1}$ [$\nu(\text{CH}_3)$] and 1469 [$\delta(\text{CH}_3)$], and 1361 cm^{-1} [$\delta(\text{CH}_3)$] (Figure S1a). In contrary, the FT-IR spectrum of (**3-med**) shows only a slight decrease of the intensity of the $\nu(\text{OH})$ band at 3749 cm^{-1} , because around 60 % of $[\equiv\text{SiOH}]$ remain unreacted. The vibrational stretching of the methyl ligand appears in the region between $3081\text{-}2819\text{ cm}^{-1}$ and the deformation bands at 1412 cm^{-1} [$\delta(\text{CH}_3)$].

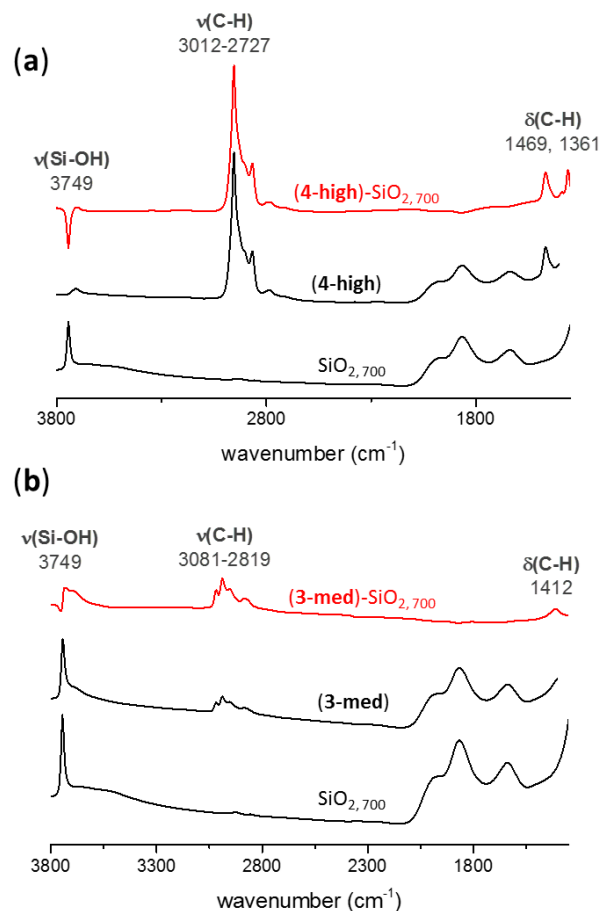


Figure S1. FTIR spectra of $\text{SiO}_{2,700}$, **(4-high)** and the subtraction **(4-high)** - $\text{SiO}_{2,700}$ (red) in the 3900–1400 cm^{-1} region at 25 °C (a); and FTIR spectra of $\text{SiO}_{2,700}$, **(3-med)** and the subtraction **(3-med)**- $\text{SiO}_{2,700}$ (red) in the 3900–1400 cm^{-1} at 25 °C (b).

4. Elemental analyses and inductively coupled plasma optical emission spectrometry (ICP-OES)

Analyses were performed at Mikroanalytisches Labor Pascher (Germany). Additionally, the titanium, zirconium, tungsten, zinc and gallium content were determined on Varian 720-ES ICP-Optical Emission Spectrometer after the samples preparation by microwave digestions ($\text{HCl}:\text{HNO}_3$, 3;1 (v:v) 8 mL and 1 mL HF) on and on Milestone ETHOS 1. Analyses of C and H was done on Flash 2000 Elemental Analyzer from Thermo Scientific.

5. Nitrogen adsorption/desorption measurements

The hydrophobicity of highly dehydroxylated (700°C) of functionalized and non-functionalized silica NPs was investigated by nitrogen adsorption method at cryogenic temperature (77 K).

A typical isotherm of highly dehydroxylated SiO₂₋₇₀₀ (**0**) is shown in Figure S1. It is a classical type IV isotherm, which bears a characteristic H1 hysteresis loop. A type IV isotherm indicates the monolayer adsorption followed by multilayer formation and capillary condensation.¹² Analysis of the isotherms yielded a BET surface area of the parent (**0**) of 184±5 m²/g. The surface area decreases to 170±5 m²/g, if the silanols are passivated by TMS (**0-high**). These results are in accordance with a more detailed study on silylated fumed silica revealing a decrease of the BET surface area with growing carbon loading and decreasing content of surface silanol groups.¹³

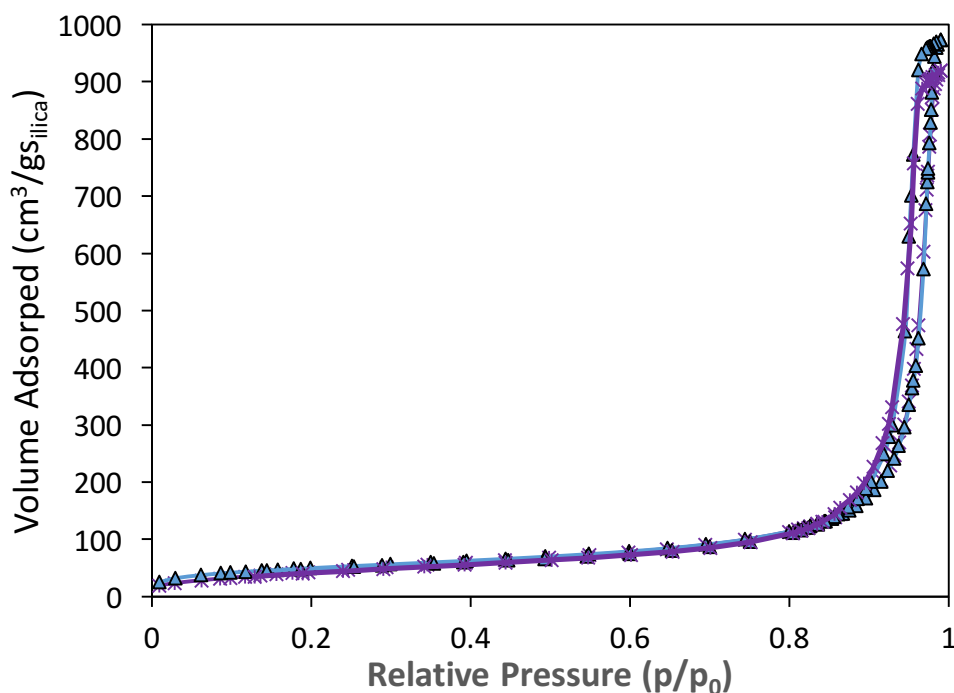


Figure S2. Nitrogen adsorption/desorption isotherms at 77 K of (**0**) – in blue - and (**0-high**) – in violet.

The C_{BET} value¹⁴⁻¹⁶ was determined according to literature from the BET analysis of the portion of the isotherm between the relative pressure (p/p_0) of 0.05 and 0.20 according to the following equation (1):

$$C_{BET} \approx \frac{V_{ads}}{p/p_0} + V_{ads} \quad (1)$$

where V_{ads} is the quantity of gas adsorbed per unit adsorbent mass and p/p_0 is the ratio of the pressure at adsorption equilibrium.

6. Transmission-electron microscopy (TEM)

A microscope of model Tecnai G2 Spirit TWIN, a 20-120 kV/LaB6 was employed. Experiments are limited to non-reactive silica NPs (**0**) and TMS-covered silica NPs (**0-high**). Particles were dispersed for 1 h at 40 °C in a hydrophobic epoxy resin (EPON¹⁷, 30 mg/mL resin)¹⁸ and then polymerized at 60 °C for 20 h. Several different sections of **0** and **0-high** were investigated by TEM where the size of silica aggregates were measured. An average aggregate size was determined based on 182 (**0**) and 129 particle counts (**0-high**), respectively. Significant morphological and structural particularities of both samples **0** and **0-high** in epoxy coats can be found in Figure S3. Unmodified silica particles **0** have a strong tendency to aggregate in epoxy coat while the modified silica particles **0-high** are homogeneously dispersed in the epoxy matrix indicating the improved compatibility of TMS-modification silica with epoxy resin. Moreover, the particle distribution highlights the impact of the organosilyl-functionalization on the dispersion behavior of the nanoparticles. While **0** has a broad average size distribution between 10 to 2000 nm with 40% of all particles having a hydrodynamic radius between 100-500 nm. Contrary, for TMS-functionalized NPs **0-high**, the average is narrower with 80% of the average aggregate radius ranging from 10 and 100 nm.

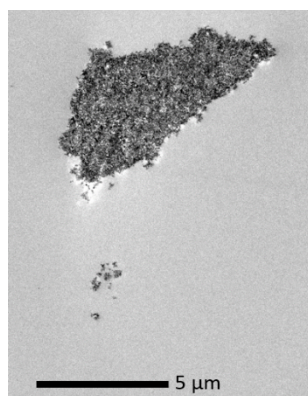


Figure S3. The TEM micrograph and histogram of particle size distribution of (a) unmodified **0** and (b) modified silica NPs **0-high** dispersed in epoxy matrix. Particles were measured with a resolution between 1.2 and 0.128 pixel/nm. The histogram of **0** is based 182 particle counts; the one for **0-high** is based on 129 particle counts.

7. Computational Methods

To evaluate the aggregation of passivated and non-passivated silica nanoparticles, we performed molecular dynamics simulation to obtain the free energy as a function of distances between the geometry centers of two silica particles. The empirical force field parameters were obtained from previous simulations of silica particles.¹⁹ All the missing parameters for functionalized silica or *o*-DCB solutions were obtained from the OPLS force field.²⁰ In practice, we constructed three silsesquioxane models.

As a model for silica nanoparticles ($d_{\text{particle}} \sim 120 \text{ \AA}$) **0**, which we used for our studies, the silsesquioxane T₈-cage (SiO_{1.5}(OH))₈ ($d_{\text{particle}} \sim 8.7 \text{ \AA}$) bearing eight [≡SiOH] groups (**M-0**). The model **M-0** was functionalized alternated with four 2,2,6,6-tetramethyl-4-neopentylheptan-4-yl (C(CH₂-^tBu)₃) groups (**M-CH₂-ⁱBu**) serving as a model for **1-med**, **2-med**, **4-med** and with four ^tBu (CMe₃) groups (**M-Me**) representing **3-med** (Figure S4).

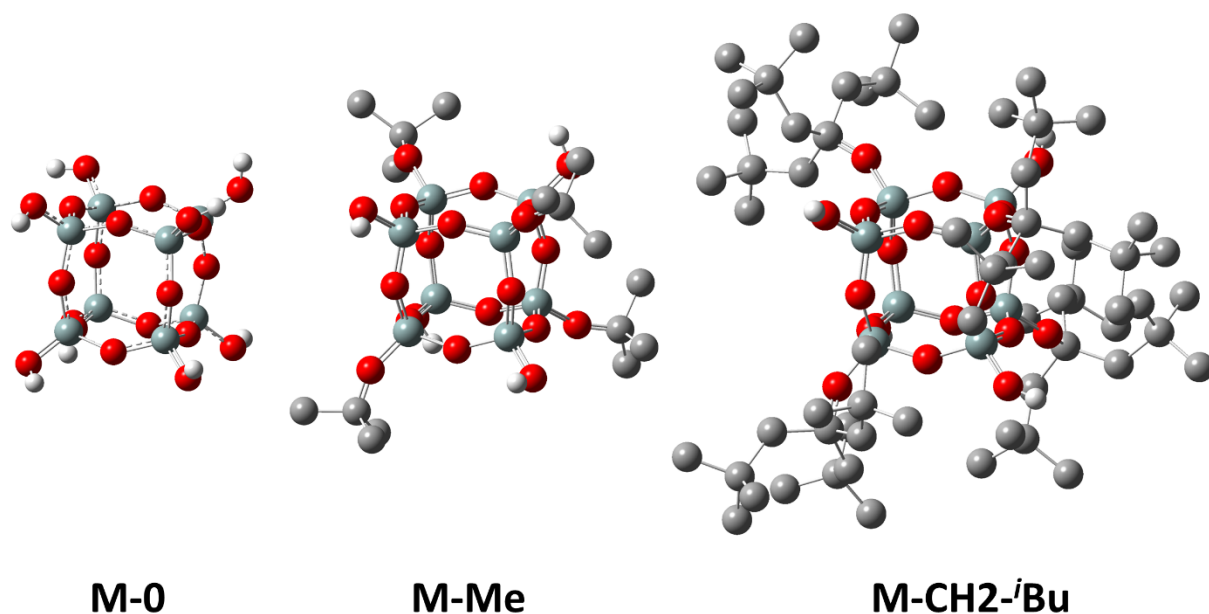


Figure S4. Silsesquioxane models representing silica-NPs **0** (**M-0**), silica-NPs covered with small ligands (**M-Me**) and silica NPs covered with larger ligands (**M-CH₂-^tBu**).

Two silsesquioxane-particles having the same functionalization were put into a *o*-DCB solution consisting of 3375 solvent molecules. The systems were pre-equilibrated in the NPT ensemble²¹ at 300 K and 1 atm for 5 ns. Then, umbrella sampling method was employed to calculate the potential of mean force as a function of distances between two particles, ranging from 8 to 25 \AA . Each simulated system consists of

17-18 windows depending of the diameter of the silica particle. A 5 kcal/mol·Å² spring were added to each window to constrain the distances. To obtain a converged result, each window was simulated in the NPT ensemble for 30 ns, and the last 25 ns trajectory was used to calculate the potential of mean force (PMF).

For the fully hydroxide system, a relative deep well at 8.3 Å was observed. This well corresponds to the direct contact of two silica particles with several hydrogen bonds formed between them. A second shallower minimum at 10.3 Å was also observed, corresponding to two silsesquioxanes having their top site contacting each other and forming one hydrogen bond. If half of the silanols are passivated with *t*-butyl-groups (**M-Me**), the first minimum disappears, and the second minimum (*vide infra*) is shifted due to the functionalization. This effect is clearer with **M-CH₂^tBu** bearing a much larger bulky functionalization on the silica-silanol. Such trend is consistent with experimental observation that the silica NPs **0** can easily aggregate in the *o*-DCB solution, while a full passivation of the [SiOH] group with bulky substituents (as **4-high**) hinders this aggregation and facilitates a better dispersion of the silica nanoparticles in non-polar solvent.

8. Dynamic Nuclear Polarization Surface Enhanced NMR spectroscopy (DNP SENS)

DNP enhanced solid-state NMR experiments were conducted on a 400 MHz Bruker Avance III DNP solid-state NMR spectrometer using a 3.2 mm Bruker triple resonance low temperature magic angle spinning (LTMAS) probe. The experiments were performed at *ca.* 100 K with a 263 GHz MW irradiation. The sweep coil of the main magnetic field was set for the microwave irradiation occurring at the ¹H positive enhancement maximum of the TEKPol biradical.

Sample Preparation. 40 μL of a biradical solution consisting of 16 mM TEKPol in 1,2-dichlorobenzene (DCB) ($c_{\text{TEKPol}} = 0.6 \mu\text{mol}_{\text{TEKPol}}/\text{sample}$ corresponding to a radical concentration $c_{\text{radical}} = 1.2 \mu\text{mol}_{\text{radical}}/\text{sample}$) was used for impregnating 20 mg of finely ground SOMC catalysts (corresponding to a loading between 1 and 5 μmol/sample). Hence, the [SOMF]/[radical]-ratio will be always ≥ 1 (Table S1). This implies that assuming that [SOMF] are fully accessible at all loadings (**low**, **med** and **high**), all polarization agent should be deactivated and no ¹H enhancement ϵ_{H} should be observed. If this is not the case ϵ_{H} should be obtained. In a typical experiment, the sample was packed into a sapphire rotor capped with a Teflon plug under argon atmosphere and then immediately inserted into the pre-cooled DNP probe for experiments.

Table S1. SOMF and TEKPol concentrations for DNP experiment using 20 mg of SOMF and 40 μ L of 16 mM TEKPol solution in *o*-DCB.

material	[SOMF] (μ mol)	TEKPol (μ mol)	[SOMF]/[radical]
0	-	0.6	-
1-med	3.6	0.6	3.0
2-med	3.1	0.6	2.6
3-med	2.5	0.6	2.1
3-low	1.4	0.6	1.2
4-high	4.7	0.6	3.9
4-med	2.3	0.6	1.9
4-low	1.4	0.6	1.2
5-med	2.1	0.6	1.8

Technical Details. The probe configuration used triple mode for ^1H , ^{13}C and ^{29}Si nuclei. The amplitude of ^1H spin lock was ramp 100.50.100 to have the maximum value. DNP enhancement factors (ϵ) were measured by integrating the intensity of spectra acquired with and without continuous wave irradiation. For ^{13}C NMR experiments the acquisition parameters used are 3 s repetition delay, a ^1H $\pi/2$ pulse length of 2.5 μ s to afford 100 kHz ^1H decoupling using the SPINAL 64 decoupling method.

A 2 ms contact time was used for cross polarization experiments. The MAS frequency varied between 8 and 10 kHz. All ^{13}C NMR spectra were referenced to adamantane with the higher frequency peak set to 38.48 ppm with respect to TMS (0 ppm).

The two-dimensional (2D) ^1H - ^{13}C heteronuclear correlation (HETCOR) spectra was acquired with 208 scans per t_1 increment, 96 individual increments and 2 ms contact time. During t_1 , e-DUMBO-1 homonuclear ^1H decoupling was applied and proton chemical shift were corrected by applying a scaling factor of 0.57.²²

8.1. DNP SENS experiments

Results of SOMF **3** were compared with literature values, where the SOMF is protected from a reaction with TEKPOL inside the mesopores of silica (**3-MCM41** – 6.2 wt.% of W)²³ and are shown in Figure S5. For **3-low**, it was possible to detect two characteristic non-equivalent methyl-signals at 71 and 91 ppm after

1570 scans, however with low S/N-ratios. For **3-med** (2.3 wt.% of W) only 288 scans were needed leading to ^{13}C CP DNP SENS with high quality comparable to **3-MCM41**.²³

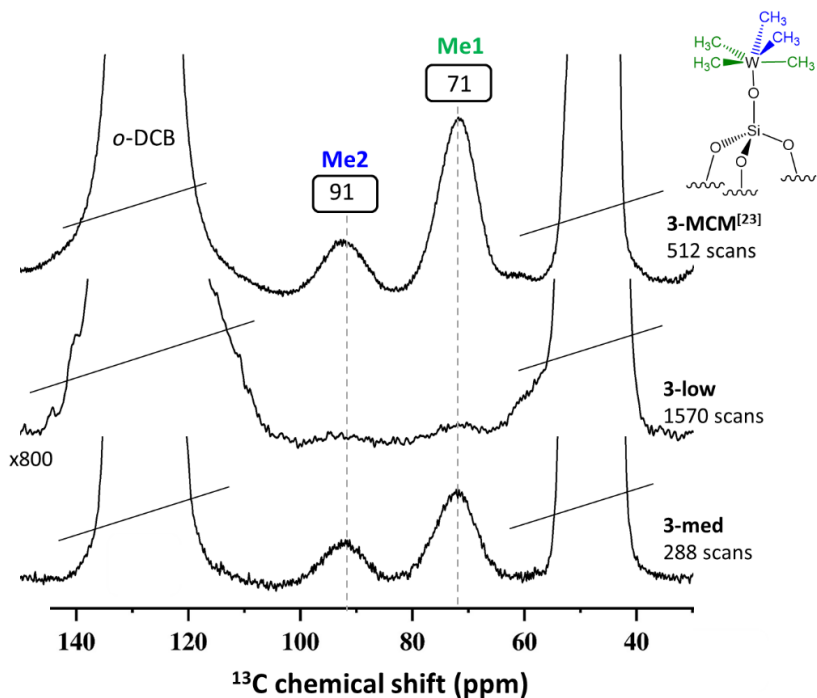


Figure S5. ^{13}C CP MAS DNP SENS spectra (100 K, 400 MHz / 263 GHz) of **3-MCM41** and **3-low**, **3-med** in a 16 mM TEKPol solution in *o*-DCB. The MAS frequency was 8 kHz. Characteristic resonances were obtained after 512 scans (**3-MCM41**),²³ 1570 scans (**3-low**) 288 scans (**3-med**).

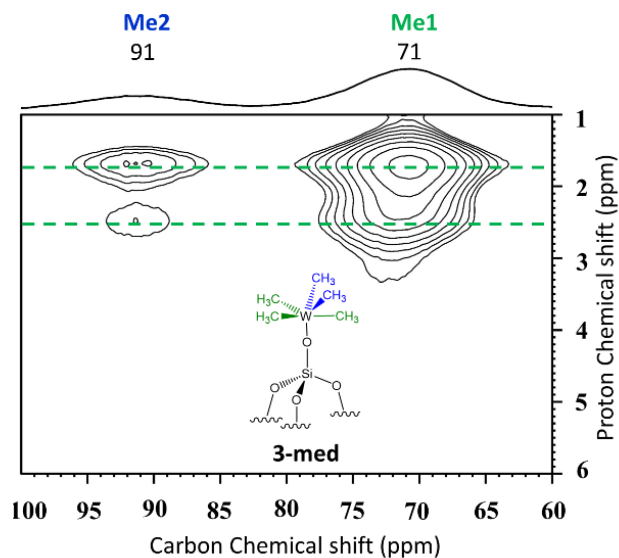


Figure S6. ^1H - ^{13}C HETCOR DNP SENS spectra (100 K, 400 MHz/ 263 GHz gyrotron) of **3-med** in 16 mM TEKPol o-DCB solution obtained at a 8 kHz MAS frequency. The green line represents the correlation of ^1H and ^{13}C signal.

A ^1H - ^{13}C HETCOR DNP SENS spectrum could be recorded in 10 h (Figure S6). All typical characteristic signals of **3-med**²³ could be detected and are highlighted by the green lines.

The DNP SENS for **4** at various concentrations are shown in Figure S6 and also compares to literature results.²³ For **4-low**, it was very challenging to obtain the SOMF-signals, even though detecting a reasonable solvent ϵ_{H} of 65. After 20 000 scans, only very weak signals at 31 ppm [$\text{W-CH}_2\text{C}(\text{CH}_3)_3$] and at 95 ppm [$\text{W-CH}_2\text{C}(\text{CH}_3)_3$] appeared. The weak signals might be due to strong hydrogen bonding between silica nanoparticles leading to 3D networks which do not allow solvent molecules in the interparticular space. Hence the transfer of polarization is weak.

For **4-med**, [$\text{W-CH}_2\text{C}(\underline{\text{C}}\text{H}_3)_3$]-signals at 31 ppm (S/N-ratio of 28) and a [$\text{W-CH}_2\text{C}(\text{CH}_3)_3$]-signal appeared at 95 ppm after 16 000 scans. Note that due low W-loading of **4-med** (2.1 wt-% W) compared to **4-MCM41** (5.7 wt% of W), the lesser intense quaternary carbons were not detected).

For **4-high**, no enhancement could be detected indicating a complete destruction of TEKPol.

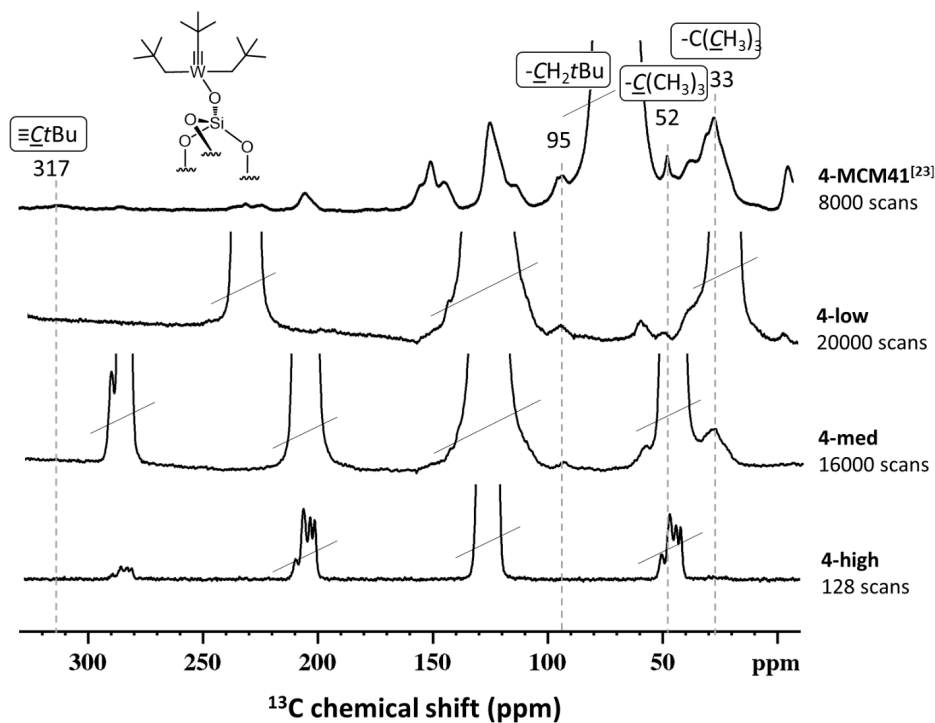


Figure S7. ^{13}C CP MAS DNP SENS spectra (100 K, 400 MHz / 263 GHz) of **4-MCM41**²³ in a 16 mM TEKPol solution in TCE and **4-low**, **4-med** and **4-high** in a 16 mM TEKPol solution in *o*-DCB. The MAS frequency was 8 kHz (**4-MCM41**, **4-med** and **4-high**) and 10.5 kHz (**4-low**). Characteristic resonances were obtained after 8000 scans (**4-MCM41**), 20000 scans (**4-low**) 16000 scans (**4-med**). No characteristic resonances were obtained for **4-high** (128 scans).

8.2. Build up time

The DNP build up time with microwave irradiation ($T_{B,on}$) was measured. Proton and carbon spin lattice relaxation were obtained using a saturation recovery experiment. Data are fit using a stretched exponential, where, A_{on} is the equilibrium normalized signal at μ wave on, $S(\tau)$ is the intensity of the signal at the polarization time τ , and β is the stretching parameter and T_B value is the observed signal build-up time.

$$S(\tau) = A_{on} \left[1 - \exp\left(-\left(\frac{\tau}{T_{B,on}}\right)^\beta\right) \right]$$

Table S2. Summary of ^{13}C relaxation measurements for *o*-DCB in **3-low**, **3-med**, **4-low**, and **4-med** with 16 mM TEKPol in *o*-DCB acquired with microwave irradiation.^a

	3-low	4-low	3-med	4-med
$A_{\text{on (au)}}$	1.0	1.0	1.0	1.0
$T_{\text{B, on (s)}}$	4.9	9.3	6.1	18.7
β	1.0	1.0	0.7	1.0

^aIntegrated signal is simulated with 95% confidence bounds.

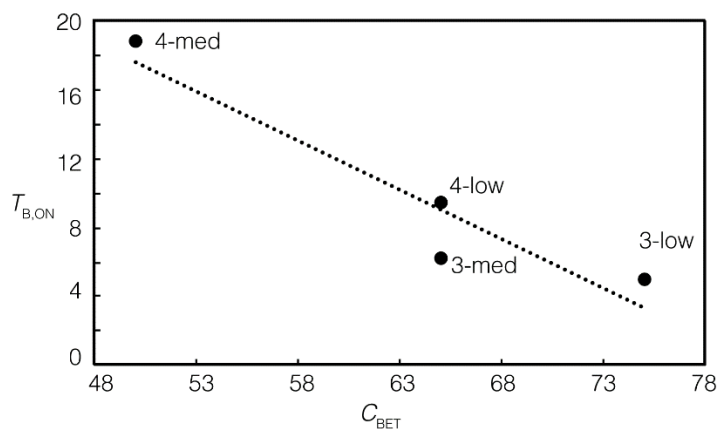


Figure S8. Plot of the build-up time with μwave on ($T_{\text{B,ON}}$) of *o*-DCB as a function of C_{BET} .

To obtain more information about the polarization mechanism of SOMFs, ^{13}C saturation recovery experiments with μwave on were measured for the solvent *o*-DCB. The build-up curves were fitted with stretched exponential functions and values may be found in Table S2. The radical solvent, *o*-DCB, build-up time on ($T_{\text{B,ON}}$) increases with decreasing of C_{BET} for the various samples (see Figure S7). This is in line with the formation of aggregates which can be thought of domains. In the presence of a domain, the radical is outside in the solution *o*-DCB. The enhancement of the solvent will be higher and the build-up time will be short due to its proximity to the radical. If no domains are formed (low C_{BET} value), then the radical concentration decreases as it interacts with the SOMFs. The radical and SOMF will react this means that the observed enhancement of the solvent will be smaller than in bulk solution, and the build-up time of the solvent will increase.

Table S3. Summary of ^{13}C relaxation measurements for **3-med** with 16 mM TEKPol in *o*-DCB acquired with microwave irradiation ($\mu\text{wave on}$).^a

	Me1	Me2	<i>o</i> -DCB
$\delta(^{13}\text{C}) / \text{ppm}$	71(24)	91(4)	130(12)
$A_{\text{on (au)}}$	1.0	1.0	1.0
$T_{\text{B, on (s)}}$	2.2	2.4	6.1
β	0.8	0.8	0.7

^aIntegrated signals are simulated with 95% confidence bounds.

9. EPR spectroscopy

EPR experiments were performed on a Bruker EMXplus-10/12 CW EPR spectrometer equipped with high sensitivity resonator. Samples were prepared the same way as for DNP SENS experiments: 20 mg silica were impregnated with 40 μL 16 mM TEKPol in *o*-DCB and sealed in NMR rotors. The rotor was then put in an EPR tube and the samples were measured at 25 $^{\circ}\text{C}$.

TEKPol concentrations were calculated using Bruker SpinCount quantification package.

Table S4. TEKPol spin counts and concentrations of **0** and **4-high** after 1 hour and 4.5 hours

Material	0	4-high
Weight, mg	14.12	17.41
Spincount after 1 h	3.976×10^{17}	3.14×10^{16}
TEKPol concentration after 1 h, nmol/mg _{sample}	23.4	1.5
Spincount after 4.5 h	3.642×10^{17}	8.492×10^{15}
TEKPol concentration after 4.5 h, nmol/mg _{sample}	21.4	0.4

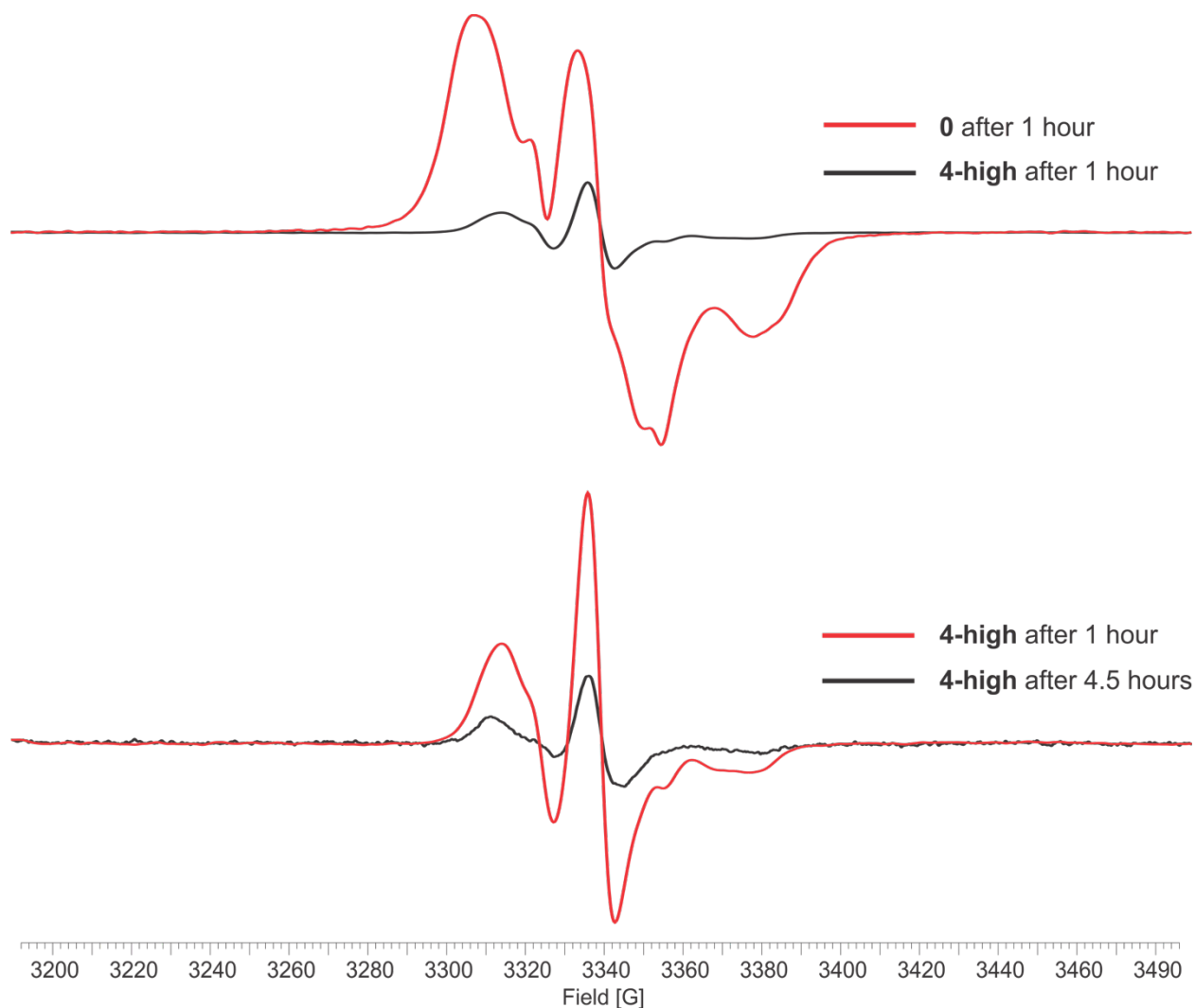


Figure S9. Normalized EPR spectra of **0** (red) and **4-high** (black) after 1 hour (upper) and EPR spectra of **4-high** after 1 h (red) and **4-high** (black) after 4.5 hours (lower).

10. References

- H. Zhu, S. Ould-Chikh, H. Dong, I. Llorens, Y. Saih, D. H. Anjum, J.-L. Hazemann and J.-M. Basset, *Chemcatchem*, 2015, **7**, 3332-3339.
- M. K. Samantaray, E. Callens, E. Abou-Hamad, A. J. Rossini, C. M. Widdifield, R. Dey, L. Emsley and J. M. Basset, *J. Am. Chem. Soc.*, 2014, **136**, 1054-1061.
- A. Shortland and G. Wilkinson, *Journal of the Chemical Society, Chemical Communications*, 1972, 318a-318a.
- R. A. Kovar, H. Derr, D. Brandau and J. O. Callaway, *Inorganic Chemistry*, 1975, **14**, 2809-2814.
- S. A. King and J. Schwartz, *Inorganic Chemistry*, 1991, **30**, 3771-3774.
- R. P. Saint-Arroman, J.-M. Basset, F. Lefebvre and B. Didillon, *Applied Catalysis A: General*, 2005, **290**, 181-190.
- A. Zagdoun, G. Casano, O. Ouari, M. Schwaerzwalder, A. J. Rossini, F. Aussenac, M. Yulikov, G. Jeschke, C. Coperet, A. Lesage, P. Tordo and L. Emsley, *Journal of the American Chemical Society*, 2013, **135**, 12790-12797.
- E. Le Roux, M. Taoufik, M. Chabanas, D. Alcor, A. Baudouin, C. Coperet, J. Thivolle-Cazat, J. M. Basset, A. Lesage, S. Hediger and L. Emsley, *Organometallics*, 2005, **24**, 4274-4279.

K. C. Szeto, A. Gallo, S. Hernández-Morejudo, U. Olsbye, A. De Mallmann, F. Lefebvre, R. M. Gauvin, L. Delevoye, S. L. Scott and M. Taoufik, *The Journal of Physical Chemistry C*, 2015, **119**, 26611-26619.

X.-X. Wang, L. Veyre, F. Lefebvre, J. Patarin and J.-M. Basset, *Microporous Mesoporous Mat.*, 2003, **66**, 169-179.

J. D. Webb, T. Seki, J. F. Goldston, M. Pruski and C. M. Crudden, *Microporous Mesoporous Mat.*, 2015, **203**, 123-131.

M. Thommes, K. Kaneko, A. V. Neimark, J. P. Olivier, F. Rodriguez-Reinoso, J. Rouquerol and K. S. W. Sing, *Pure and Applied Chemistry*, 2015, **87**, 1051-1069.

H. Barthel, L. Rösch and J. Weis, in *Organosilicon Chemistry II*, Wiley-VCH Verlag GmbH, 2008, pp. 761-778.

L. Jelinek and E. S. Kovats, *Langmuir*, 1994, **10**, 4225-4231.

D. Brunel, A. Cauvel, F. Di Renzo, F. Fajula, B. Fubini, B. Onida and E. Garrone, *New J. Chem.*, 2000, **24**, 807-813.

J. A. Osaheni and S. T. Buddle, *Journal*, 2001.

J. H. Luft, *The Journal of Biophysical and Biochemical Cytology*, 1961, **9**, 409-414.

J. J. Yuan, S. X. Zhou, G. X. Gu and L. M. Wu, *J. Mater. Sci.*, 2005, **40**, 3927-3932.

F. S. Emami, V. Puddu, R. J. Berry, V. Varshney, S. V. Patwardhan, C. C. Perry and H. Heinz, *Chemistry of Materials*, 2014, **26**, 2647-2658.

W. L. Jorgensen, D. S. Maxwell and J. TiradoRives, *Journal of the American Chemical Society*, 1996, **118**, 11225-11236.

S. Melchionna, G. Ciccotti and B. Lee Holian, *Molecular Physics*, 1993, **78**, 533-544.

B. Elena, G. de Paepe and L. Emsley, *Chemical Physics Letters*, 2004, **398**, 532-538.

E. Pump, J. Viger-Gravel, e. Abou-Hamad, m. samantaray, b. hamzaoui, A. Gurinov, D. H. Anjum, D. Gajan, A. Lesage, A. Bendjeriou-Sedjerari, L. Emsley and J.-M. Basset, *Chemical Science*, 2016.